



Dynamic investigation of solid propellant combustion in a rocket motor chamber

R. Gheshlaghi^a, S. Ghotbi^b, G. Zahedi^{c1}

^a Department of Chemical Engineering, Ferdosi University, Mashhad, Iran

^b Department of Chemical Engineering, Sharif University of Technology, Tehran, Iran

^c Department of Chemical Engineering, Razi University, Kermanshah, Iran, 67149

grzahedi@razi.ac.ir

Abstract

This study considers dynamic investigation of combustion phenomena in a Solid Propellant Rocket Motor (SPRM). Gas dynamic in combustion chamber and effluent nozzle has been studied by solving governing equations (mass, energy and momentum balances). In the modeling, spread of flame and variation of mass added from propellant surface into the gas stream are considered. The governing equations, which were in Euler form, were solved numerically by applying Modified Mac-Carmak method. Pressure, temperature and velocity distributions were found as a function of time and axial distance. The results were validated by experimental data of a typical rocket motor. Effects of various factors on combustion were evaluated. The proposed model can be easily modified and used for other solid propellants even with low aluminum content.

Key words: rocket motor, combustion, propellant, dynamic modeling.

1. Introduction

Performance of a SPRM is rigorously depends on flow distribution, fuel composition and temperature distribution. These parameters can be specified by variables such as pressure, temperature, velocity, density, composition in the motor and variation of cross section area. In order to investigate effect of these variables on SPRM performance detailed model of the motor is necessary.

Several researchers have studied SPRM combustion modeling. Most of the earlier work in exploring the flow evolution in a rocket chamber was based on cold-flow studies with injection of inert gases through the sidewalls of the chamber simulating the gas influx from the burning propellant. In this idealized configuration, Taylor [1] and later Culick [2] obtained analytical expressions for the velocity distributions in laminar incompressible flows. The study was later extended by Balakrishnan et al. [3] to include the effects of rotationality and compressibility. Dunlap et al. [4] and Traneau et al. [5] conducted experiments for incompressible and compressible flows, respectively, to quantify the turbulence characteristics and mean velocity transitions in the chamber. Three regimes of flow evolution: the upstream laminar, transitional, and downstream turbulent regions, were identified. Beddini [6] and Sabnis et al. [7] applied turbulence closure models to obtain numerical results of the flow field.

¹ Corresponding author: grzahedi@razi.ac.ir



Sourabh et al [8] have simulated a SPRM by means of a large eddy simulation technique. They found that chemical reaction has laminar role in combustion at slower rate and propellant combustion maybe locally treated as a well stirred reactor. Pirotti et al [9] have concluded flame speeding factor in their one dimensional modeling. Their model is pure mathematical and haven't been validated by experiments. Redulphé [10] have considered radiation in modeling of a SPRM. They have used Lagrangian approach to solve governing equations with CFD. Kim et al. [11] are divided a rocket motor into three region as solid phase, foam phase and gas phase. Conservation laws have been written for each section respectively. Jae-kun et al. [12] have employed one dimensional unsteady state models for combustion of RDX/GAP/BTTN in a rocket motor. They have adopted a rate of reaction as $r = ka^p$ from ref [13] in their modeling. They found that estimated burning rate of RDX/GAP/BTTN is in general higher than RDX/GAP alone. Their modeling responds in 1-100 atm pressure range.

The objective of current study is to provide a reliable and realistic model to analyze the combustion in SPRM. Considering erosive burning in modeling, generality of the proposed model and finally implementing artificial viscosity in numerical solution are the advantages of current article to previous researches.

2. Process Modeling

Figure 1, represents a typical SPRM chamber which is divided into three sections. Section between chamber front to $x=x_0$, entrance section, section between $x=x_0$ to $x=x_n$, propellant section, and finally nozzle section which is located between $x=x_n$ to $x=x_e$.



Fig.1. Schematic of a typical SPRM.

As hot gas enters the chamber, heats up the propellant. Propellant is ignited when a point on propellant surface reaches its critical ignition point [13]. This process continues when total amount of propellant is ignited. Because of high gas velocity and erosive burning there will be a great pressure in the chamber and by exiting gases from nozzle the ignition reaches a steady form.

2.1. Governing equations

In order to build a model for combustion phenomena the following assumptions have been used:

1. The flow is one-dimensional in the chamber. Turbulence of the gases in the chamber makes this assumption reasonable.
2. All the surface reactions take place in a thin zone near the surface (reaction surface).
3. Physical properties of igniter gas and the gases from propellant burning are the same.



4. Gases in the chamber obey perfect gas law.
 5. Viscous dissipation and axial heat conduction are assumed to be negligible.
- the conservative laws are written as:

- Continuity:

$$\frac{\partial(\rho A)}{\partial t} + \frac{\partial(\rho u A)}{\partial x} = r \rho_{pr} P_w \quad (1)$$

- Momentum:

$$\frac{\partial(\rho u A)}{\partial t} + \frac{\partial(\rho u^2 A)}{\partial x} + \frac{\partial(PA)}{\partial x} = P \frac{\partial A}{\partial x} - \tau_w P_w \quad (2)$$

- Energy :

$$\frac{\partial(EA)}{\partial t} + \frac{\partial[(E + P)uA]}{\partial x} = q_p - q_b \quad (3)$$

Where

$$q_p = r \rho_{pr} P_w h_f \quad (4)$$

$$q_b = P_w h_c (T - T_{ps}) \quad (5)$$

Equation (1) – (3) are general form of conservative equations , but for each zone of chamber the right hand side of the equations have different forms as below:

One) $x_i < x < x_n$

- $T_{ps} < T_{ps,ig}$

In this case there is no ignition and the equations will have the following form:

$$\frac{\partial(\rho A)}{\partial t} + \frac{\partial(\rho u A)}{\partial x} = 0 \quad (6)$$

$$\frac{\partial(\rho u A)}{\partial t} + \frac{\partial(\rho u^2 A)}{\partial x} + \frac{\partial(PA)}{\partial x} = P \frac{\partial A}{\partial x} - \tau_w P_w \quad (7)$$



$$\frac{\partial(EA)}{\partial t} + \frac{\partial[(E + P)uA]}{\partial x} = -q_b \quad (8)$$

- $T_{ps} \geq T_{ps,ig}$

$$\frac{\partial(\rho A)}{\partial t} + \frac{\partial(\rho u A)}{\partial x} = r \rho_{pr} P_w \quad (9)$$

$$\frac{\partial(\rho u A)}{\partial t} + \frac{\partial(\rho u^2 A)}{\partial x} + \frac{\partial(PA)}{\partial x} = P \frac{\partial A}{\partial x} - \tau_w P_w \quad (10)$$

$$\frac{\partial(EA)}{\partial t} + \frac{\partial[(E + P)uA]}{\partial x} = q_p \quad (11)$$

Two) $x_n < x < x_e$

$$\frac{\partial(\rho A)}{\partial t} + \frac{\partial(\rho u A)}{\partial x} = 0 \quad (12)$$

$$\frac{\partial(\rho u A)}{\partial t} + \frac{\partial(\rho u^2 A)}{\partial x} + \frac{\partial(PA)}{\partial x} = P \frac{\partial A}{\partial x} - \tau_w P_w \quad (13)$$

$$\frac{\partial(EA)}{\partial t} + \frac{\partial[(E + P)uA]}{\partial x} = 0 \quad (14)$$

2.2. Initial and boundary conditions

To solve equations (6)-(14) three initial conditions are necessary. These conditions which are the same for all location of chamber are:

$$u(0,x) = u_i \quad (24)$$

$$T(0,x) = T_i \quad (25)$$

$$P(0,x) = P_i \quad (26)$$

Where u_i , T_i and P_i are initial velocity, temperature and pressure of the chamber. In order to avoid numerical difficulties P_i are assumed to be 0.0001 greater than atmospheric pressure. At exit section P_e is equal to ambient pressure and $T(t,x_e) = T(t,x_e-dx)$, $u(t,x_e) = u(t,x_e-dx)$. At interface sections Mach number, pressure and temperatures are equal. Boundary condition at $x = x_0$ are the same as exit section.



2.3. Auxiliary Equations

2.3.1. Heat transfer coefficient

Convective heat transfer coefficient has been calculated from Dittus-Bolter equation [14]. In this equation gas properties are calculated in average film temperature (T_{af}).

$$h_c = 1.56 * 10^{-3} * Pr^{-0.6} C_p (\rho u / R)^{0.8} * M_w^{0.1} * T_{af}^{-0.67} * \left(\frac{X}{d}\right)^{-0.1} \left(\frac{A_p}{A_t}\right)^{0.4} \quad (27)$$

2.3.2. Friction factor

Colebrook correlation for turbulent flow has been used for friction factor calculation. Entrance region effects are also considered in this equation [15]. All properties in this equation are calculated at T_{af} .

$$f = \frac{0.449 * \left(\frac{d}{X}\right)^{0.1}}{\left\{ \ln \left[\frac{(\varepsilon / d)}{3.7} + \frac{1.27 * R * M_w^{0.5} * T_{af}^{1.65} * \left(\frac{d}{X}\right)^{0.5}}{10^6 * P * u * d * f^{0.5}} \right] \right\}^2} \quad (28)$$

2.3.3. Burning rate

The burning rate has been adopted from Modified Lenoir-Robillard law [16]. In this equation effect of erosive burning is considered as:

$$\dot{r} = aP^n + kh_c \exp\left(\frac{-\beta \dot{r} \rho_{pr}}{\rho u}\right) \quad (29)$$

β was calculated experimentally from water-quench experimentation.

2.3.4. Propellant surface temperature before ignition

Propellant surface temperature before ignition increase, because of hot igniter gases. The temperature is described by the following equation by implementing heat conservation law across propellant thickness as:

$$\frac{\partial T_{pr}(t, y)}{\partial t} = \alpha_{pr} \frac{\partial^2 T_{pr}(t, y)}{\partial y^2} \quad (30)$$

Where

$$T_{pr}(0, y) = T_{pi} \quad (31)$$

$$T_{pr}(t, \infty) = T_{pi} \quad (32)$$

$$\frac{\partial T_{pr}(t, 0)}{\partial y} = -\frac{hc(t)}{\lambda_{pr}} [T(t) - T_{ps}(t)] \quad (33)$$

Equation (30) was solved by assuming a three order polynomial for $T_{pr}(y)$. The following ODE was obtained by inserting the polynomial.



$$\frac{\partial T_{ps}}{\partial t} = \frac{4\alpha_{pr} h_c^2 (T - T_{ps})^3}{3\lambda_{pr}^2 (T_{ps} - T_{pi})(2T - T_{ps} - T_{pi})} \quad (34)$$

In order to avoid singularity at time zero, initial condition for equation (34) is described as:

$$T_{ps}(0) = T_{pi} + \varepsilon \quad (35)$$

Where ε is a small number like 0.1 K.

3. Numerical Solution

Equations (6)-(29) and equation (34)-(35) should be solved simultaneously. In order to solve the equations Modified Mac-Cormak (MMC) method has been used [17]. This method is a predictor corrector solution for the following equation:

$$\frac{\partial U}{\partial t} + \frac{\partial E}{\partial x} = S \quad (36)$$

Where predictor equation is:

$$U_i^{\overline{n+1}} = U_i^n - \frac{\Delta t}{\Delta x} (E_{i-1}^n - E_i^n) + \Delta t * S_i^n \quad (37)$$

And corrector equation has the following form:

$$U^{n+1} = \frac{1}{2} [U_i^n + U_i^{\overline{n+1}} - \frac{\Delta t}{\Delta x} (E_i^{\overline{n+1}} - E_{i-1}^{\overline{n+1}}) + \Delta t * S_i^{\overline{n+1}}] \quad (38)$$

Equations (6)-(29) can be written in the form of equation (38) by defining U,S and E in the following vector forms:

$$U = \begin{bmatrix} \rho A \\ \rho u A \\ EA \end{bmatrix} \quad (39)$$

$$E = \begin{bmatrix} \rho u A \\ (u^2 \rho + P) A \\ (E + P) u A \end{bmatrix} \quad (40)$$

$$S = \begin{bmatrix} \dot{r} \rho_{pr} P_w \\ P \frac{\partial A}{\partial x} - \tau_w P_w \\ q_p - q_b \end{bmatrix} \quad (41)$$

Vector S for each region of the chamber will have different values based on section 2.1. The following procedure is used to solve the equation according MMC method:

1. Using quantities values at time n, the value of U,E and S at this time are known.
2. Use Eq. (38) to calculate U at time $\overline{n+1}$.
3. Using $U_i^{\overline{n+1}}$, calculate T,P, ρ and u at time $\overline{n+1}$.
4. Using quantities at time $\overline{n+1}$ and equation (40) and (41) calculate E and S at time $\overline{n+1}$.
5. Calculate U^{n+1} by replacing new quantities in Eq. (37).



6. Calculate quantities T,P, ρ and u at time n+1 from Eq. (39).

This procedure continues when the desired time is reached. In order to quarantine stability of the solution Mac Camak and Baldwin have considered the following fourth order equation called Artificial Viscosity (AV):

$$\varepsilon_e (\Delta x)^4 \frac{\partial}{\partial x} \left[\frac{|u|+a}{4P} * \left| \frac{\partial^2 P}{\partial x^2} \right| * \frac{\partial u}{\partial x} \right] \quad (42)$$

The AV is added to numerical equation as:

$$U_i^{\bar{n}+1} = U_i^n - \frac{\Delta t}{\Delta x} (F_{i-1}^n - F_i^n) + \Delta t * S_i^n \quad (43)$$

$$U^{n+1} = \frac{1}{2} [U_i^n + U_i^{\bar{n}+1} - \frac{\Delta t}{\Delta x} (F_{i-1}^{\bar{n}+1} - F_i^{\bar{n}+1}) + \Delta t * S_i^{\bar{n}+1}] \quad (44)$$

Where

$$F_i^n = E_i^n + A_i^n \quad (45)$$

$$F_i^{\bar{n}+1} = E_i^{\bar{n}+1} + A_i^{\bar{n}+1} \quad (46)$$

$$A_i^n = \varepsilon_e [(|u_i|^n + a_i^n) * \frac{|P_{i+1}^n - 2P_i^n + P_{i-1}^n|}{P_{i+1}^n + 2P_i^n + P_{i-1}^n} (U_i^n - U_{i-1}^n)] \quad (47)$$

$$A_i^{\bar{n}+1} = \varepsilon_e [(|u_i|^{\bar{n}+1} + a_i^{\bar{n}+1}) * \frac{|P_{i+1}^{\bar{n}+1} - 2P_i^{\bar{n}+1} + P_{i-1}^{\bar{n}+1}|}{P_{i+1}^{\bar{n}+1} + 2P_i^{\bar{n}+1} + P_{i-1}^{\bar{n}+1}} (U_i^{\bar{n}+1} - U_{i-1}^{\bar{n}+1})] \quad (47)$$

For stability purposes ε_e should be between 0 and 0.5. The AV is more important in the regions with pressure oscillation. Matlab version 7 has been employed to implement numerical routines.

4. Experimental Rig

In order to validate the model a typical jet motor was used. Table 1 shows the specification of the motor. Solid propellant physical properties are tabulated in Table 2.

Table 1. Characteristics of jet motor.

Quantity	Value
Entrance length	6.2 cm
Fuel section length	50 cm
Cross section area of fuel section	1.61 cm ²
Wetted perimeter	6.35 cm

Table 2. propellant physical properties (20% PBAA-EPON, 80% AP(15 μ m 30%,180 μ m 70%))

Quantity	Quantity		
a= 0.0005	cm/s.cm	$\varepsilon_s=0.001$	
n=0.4		$\gamma= 1.24$	
$\lambda_{pr}=0.00377$	J/(cm.s.K)	$T_{psig}=700$	K
$\rho_{pr}=1.6$	gr/cm ³	k= 5.27	cm ³ .K/cal
$\alpha_{pr}=0.001875$	cm ² /s	$\beta=105$	
M=2.01	gr/gr-mol		



5. Results and Discussion

Figures (3) and (4) show pressure variation with time for entrance and exit section of the chamber respectively. Plus sign (+) on pressure indicates that to avoid singularity in numerical solutions initial pressure is taken $P=1.0001$ atm. These figures show validity of predictions. Also they represent that erosive burning is important and should be considered in modeling. Perfect gas assumption seems main source of errors in the modeling and non ideality will be considered in the future works.

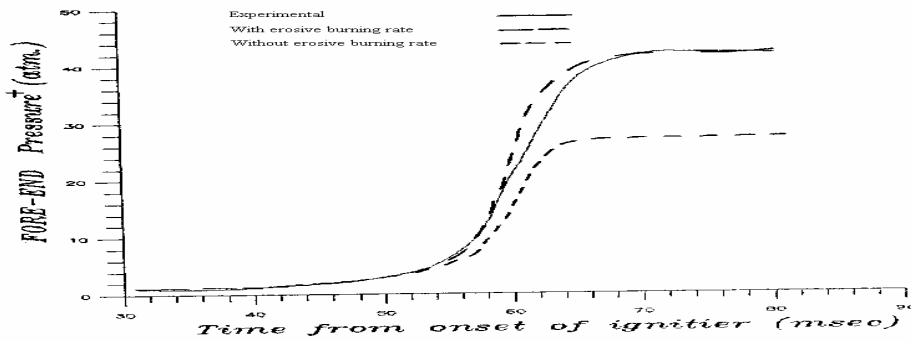


Fig.3. Pressure variation with time for entrance section of the chamber.

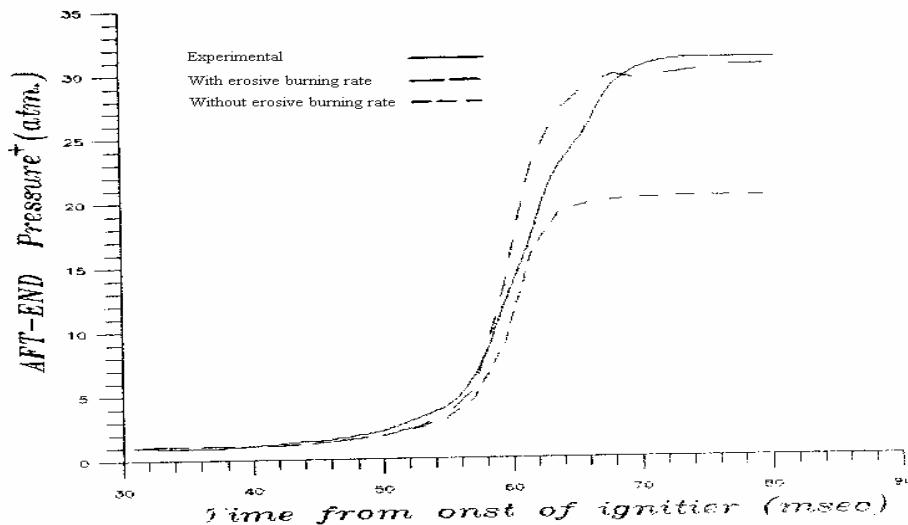


Fig.4. Pressure variation with time for exit section of the chamber.

Figure (5) represent pressure variation in combustion chamber during four different phases. At induction phase there is a good agreement between calculated and experimental results along the chamber. In flame propagation phase calculated pressure are a little bit less than experimental data. Maximum difference was observed for flame front. Calculated pressures are a little greater than experimental for chamber filling phase. In times near to steady state calculated pressures are the maximum attainable pressures in the chamber and they fit experiments.

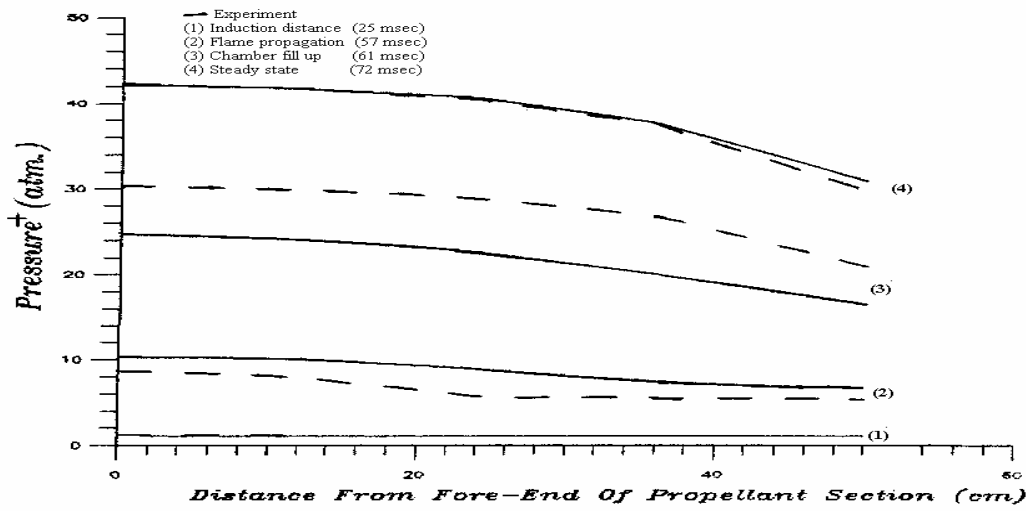


Fig.5. Pressure variation in combustion chamber during four different regimes.

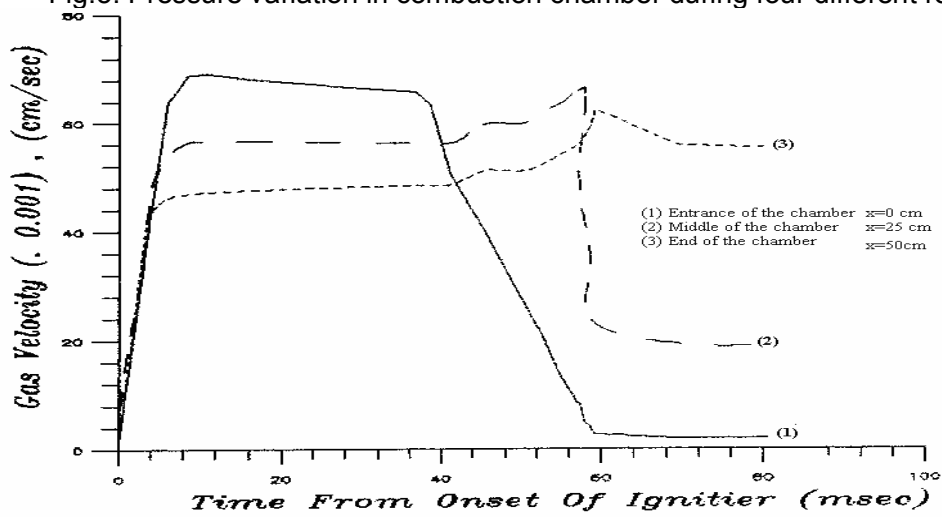


Fig.6. Gas velocity variation with time for three different zones.

Figure (6) shows gas velocity variation with time for three different chamber zones. As gas velocity increases, ignition delay decreases. Figure (7) show this fact. Increasing gas flow rate increases flame spreading time. Table 3 depicts this judgment.

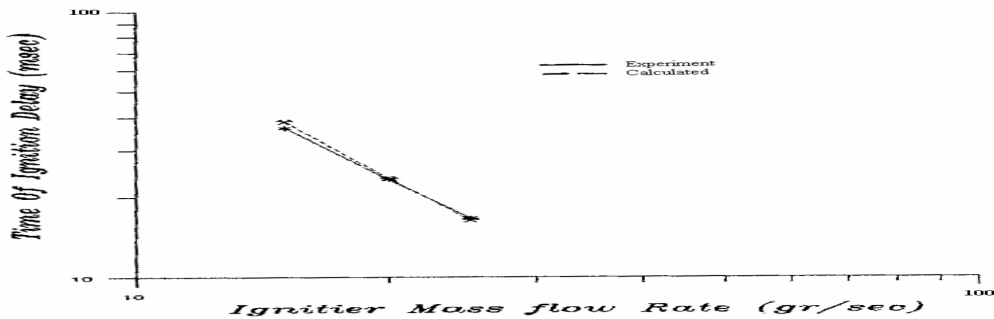


Fig.7. Dependency of ignition time with gas flow rate.

Table 3. Effect of gas flow rate on delay time.

Gas flow rate (gr/sec)	Ignition time (m sec)	End time (m sec)	Delay (m sec)
15	38.49	59.1	20.16
20	23.51	38.32	14.81

Gas flow rate also affects pressure in the chamber. Figure (8) shows that by increasing gas flow rate:

- Induction pressure increases a little.
- In propagation phase this increase is sharp.
- Time increment from flame propagation to reach maximum pressure decreases.

Table 4 shows as the ratio of A_p/A_t increases (by nozzle diameter) propagation phase starts earlier and flame spreading time decreases.

Table 4. Effect of nozzle diameter on flame spreading time and velocity.

A_p/A_t	Ignition time (m sec)	End time (m sec)	Delay (m sec)	Initial flame spreading Velocity (cm/sec)	Final flame spreading Velocity (cm/sec)
1.05	27.34	43.49	16.15	690	12500
1.20	23.56	38.28	14.72	800	14300
1.50	19.29	31.38	12.09	1020	16700

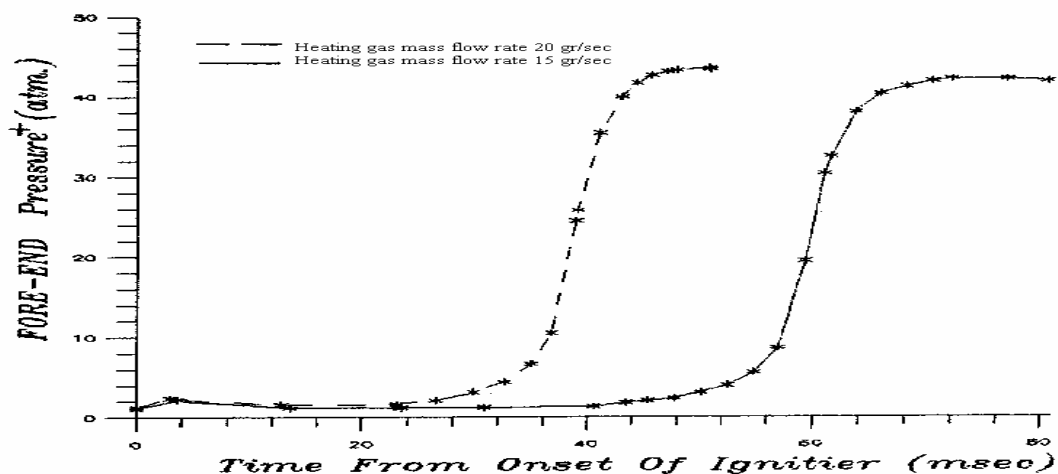


Fig.8. Dependency of Pressure with gas flow rate by the passage of time.

6. Conclusion and Remarks



In this article a model was developed to study solid-propellant jet motor by solving heat, mass and momentum conservation laws. In order to find the solution Modified Mac-Cormack method, which is stable for high pressure regions, with AV was applied to solve the equations. Results were validated with typical jet motor experimental data. Effect of operating parameters on combustion behavior was studied. The model is general and can be used for other solid propellants.

7. Nomenclature

A_p	Fuel section cross section area, cm^2
A_t	Nozzle cross section area, cm^2
a	Sound velocity, cm/sec
C_p	Heat capacity at constant pressure, erg/gr.K
C_v	Heat capacity at constant volume, erg/gr.K
D	Fuel section diameter, cm
E	Total energy, erg/gr
e	Internal energy, erg/gr
f	Friction factor
h_c	Convective heat transfer coefficient, $\text{erg/cm}^2.\text{sec.K}$
k	Coefficient of erosive burning rate, $\text{cm}^3.\text{K/cal}$
\dot{m}_{ig}	Heating gas mass flow rate, gr/sec
M	Molecular weight, gr/gr-mol
n	Pressure power index in Eq. 29
Pr	Prandtl number, cm^2/sec
P_w	Perimeter of burning, cm
q_b	Heat transferred from gas stream to fuel, $\text{erg/cm}^2.\text{sec}$
q_p	Heat transferred from flame to gas stream, $\text{erg/cm}^2.\text{sec}$
R	Universal gas constant, dyn.cm/gr.K
\dot{r}	Burning rate, gr/sec
\vec{r}	Vector in Eq. 21
T	Temperature, K
t	Time, sec
u	Gas velocity, cm/sec
x	Axial distance, cm
y	Vertical coordinate, cm

Greece letters

α	Thermal diffusivity, cm^2/sec
β	Constant of Eq. 29
γ	Ratio of heat capacities
ϵ	Small number
ϵ_e	Coefficient in artificial viscosity, Eq. 47
λ_{pr}	Conductivity of solid propellant, erg/cm.sec.K
π	Pi number
μ	Viscosity, gr/cm.sec



U
T

Kinematic viscosity, cm^2/sec
Shear stress, dyn/cm^2

Subscripts and superscripts

e
i
ig
out
pr
n
ps

Nozzle exit
Initial conditions
Heating gas
outlet
Solid propellant
Value of quantities at time n
Propellant surface



References

1. Taylor, G. I., Proceedings of Royal Society London, Series 234A, Vol. 11199, 1956, pp. 456–475.
2. Culick, F. E. C., AIAA J. 4, 1966, pp. 1462–1464.
3. Balakrishnan, G., Linan, A., and Williams, F. A., J. Propul. Power 8, 1992, pp.1167–1176.
4. Dunlap, R., Blackner, A. M., Waugh, R. C., Brown, R. S., and Willoughby, P. G., J. Propul. Power 6, 1990, pp. 690–704.
5. Traineau, J. C., Hervat, P., Kuentzmann, P., AIAA Paper 86-1447, 1986.
6. Beddini, R. A., AIAA J. 24, 1986, 1766–1773.
7. Sabnis, J. S., Madabhushi, R. K., Gibeling, H. J., and McDonald, H., AIAA Paper 89,1989, p. 2558.
8. Sourabh A. and Yang V., Unsteady Flow Evolution and Combustion Dynamics of Homogeneous Solid Propellant in a Rocket Motor, COMBUSTION AND FLAME 131, 2002, pp. 110–131.
9. D. Pierotti and Verri, M., Global classical solutions for a free-boundary problem modeling combustion of solid propellants, J. Math. Anal. Appl. 319, 2006, pp. 1–16.
10. Rodolphe Duval, Anouar Sou1ani, Jean Taine, Coupled radiation and turbulent multiphase flow in an aluminised solid propellant rocket engine, Journal of Quantitative Spectroscopy & Radiative Transfer 84, 2004, pp. 513–526.
11. E. S. KIM and V. YANG and Y.-C. LIAU, Modeling of HMX/GAP Pseudo-Propellant Combustion, COMBUSTION AND FLAME 131, 2002, 227–245.
12. Jae-Kun Yoon, Piyush Thakre, Vigor Yang, Modeling of RDX/GAP/BTTN pseudo-propellant combustion, Combustion and Flame 145, 2006, 300–315.
13. A.I. Atwood, T.L. Boggs, P.O. Curran, T.P. Parr, D.M. Hanson-Parr, J. Propuls. Power 15, 1999, 740–752.
14. Holman J.P., Heat transfer, ninth edition, chapter 6, McGraw –Hill Co., 2002, USA.
15. Colebrook, C., Turbulent flow in pipes, with particular reference to the transition regime between smooth and rough pipe laws, Institution of Civ. Eng. Journal, 11, 1939, pp. 133-156.
16. JOJIC, B. , BLAGOJEVIC, D. , Theoretical prediction of erosive burning characteristics of solid rocket propellant based on burning rate dependence of pressure and initial temperature and its energetic characteristics , American Institute of Aeronautics and Astronautics and Society of Automotive Engineers, Propulsion Conference, 12th, Palo Alto, Calif., July 1976, AIAA, p.12.
17. Jianrong Wang, Siamack A. Shirazi ,A Simultaneous Variable Solution Procedure for Laminar and Turbulent Flows in Curved Channels and Bends, Journal of Fluids Engineering, September 2000, Volume 122, Issue 3, pp. 552-559